Proceedings of the Sixth International Conference on
Railway Technology: Research, Development and Maintenance
Edited by: J. Pombo
Civil-Comp Conferences, Volume 7, Paper 3.2
Civil-Comp Press, Edinburgh, United Kingdom, 2024
ISSN: 2753-3239, doi: 10.4203/ccc.7.3.2

Energy Savings for Freight Trains with Aerodynamically Optimized Loading Schemes

A. Buhr, L. Siegel, J. Bell and A. Henning

Institute of Aerodynamics and Flow Technology
German Aerospace Center
Göttingen, Germany

Abstract

The research presented focuses on the potential of energy savings in intermodal freight rail transport by optimizing the loading scheme with regard to the aerodynamic drag. As part of this work, a parameter study was performed to quantify the effect of the loading gap size upstream and downstream of a test container on the drag of the test container itself. The resulting drag database was used to calculate the combined drag of different loading schemes and estimate the energy saving potential by reducing gaps. Within the scope of this work, wind-tunnel experiments were performed to investigate more than 200 model configurations at a yaw angle of 0° to provide a detailed look-up table for the aerodynamic drag. Measurements of selected loading schemes were repeated at a yaw angle of 5° to include crosswind effects and allow predictions for operational scenarios under realistic environmental conditions. The experiments were performed in the Crosswind Simulation Facility at DLR Göttingen at a Reynolds number of 5.0×10^5. The outcome of this work is an estimation tool for drag related energy savings, which provides information for freight train operators to carry out a cost-benefit analysis and crucial wagon design aspects for aerodynamically optimized loading schemes.

Keywords: freight train, loading scheme, aerodynamic drag, energy efficiency, estimation tool, wind tunnel test, crosswind simulation facility

1 Introduction

With the ever-increasing demand for energy efficient, low-emission freight transport, the expansion and development of rail freight transport becomes a more and more relevant topic. The average CO_2 emissions of freight trains with 16 g/t·km is multiple times lower compared to the emission of freight transport on trucks with 118 g/t·km [1]. With the need for a climate-friendly means of transport for an increasing amount of goods over land, the demand of higher freight train's capacity, speed and time-optimized logistical processes increases. Other than in the high-speed passenger train sector, the design developments of freight trains were mostly limited to structural or logistical aspects in the past. Especially the optimization of logistical processes like commissioning for different destinations can lead to significant gaps of one or multiple missing containers in the overall loading scheme. As can be imagined from Figure 1, scattered loading schemes are highly affecting the overall aerodynamic drag of a freight train. The crucial information for train operators at this point is if there are certain limits to critical gap sizes and what is the estimated, quantitative effect of these loading gaps on the total energy consumption.

Figure 1: Large gaps in the loading scheme of a freight train due to missing containers (Oberwesel, taken by K. Ehrenfried, DLR)

Previous studies in freight rail research have already shown the high potential of reducing the total aerodynamic drag of a freight train by rearranging the loads to a close-packed scheme [2],[3]. The added value of this work is a detailed parameter study for the quantitative effect of the gaps around a test container in a specific loading scheme on the drag force. The aerodynamic effect was investigated to highlight the existence of critical gap sizes, so-called regimes, which lead to a significant change in the drag. The objective of this work is to provide an incremental database to allow calculations for the total drag of the load and therefore the difference in energy consumption of a freight train with a specific loading scheme compared to a closed-packed scheme with minimal gaps.

From the train operator's perspective, the main impact of this research project is a databased tool to estimate loading scheme related energy and cost savings and information about characteristic gap regimes which should be considered in future wagon designs – especially in consideration of high-speed freight rail. The presented, quantitative analysis of the energy consumption enables the train operators to carry out a cost-benefit analysis, considering the logistical effort associated with certain aerodynamic optimisations.

2 Methods

2.1 Experimental setup

The experimental investigations were carried out in the crosswind simulation facility Göttingen (SWG), a closed-circuit, Göttingen-type wind tunnel. The test section of the SWG (Figure 2, blue) is 2.4 m wide, 1.6 m high and 9 m long. Further modifications can be set up in the test-section to improve aerodynamic investigations of ground-based vehicles at wind flow speeds up to 60 m/s.

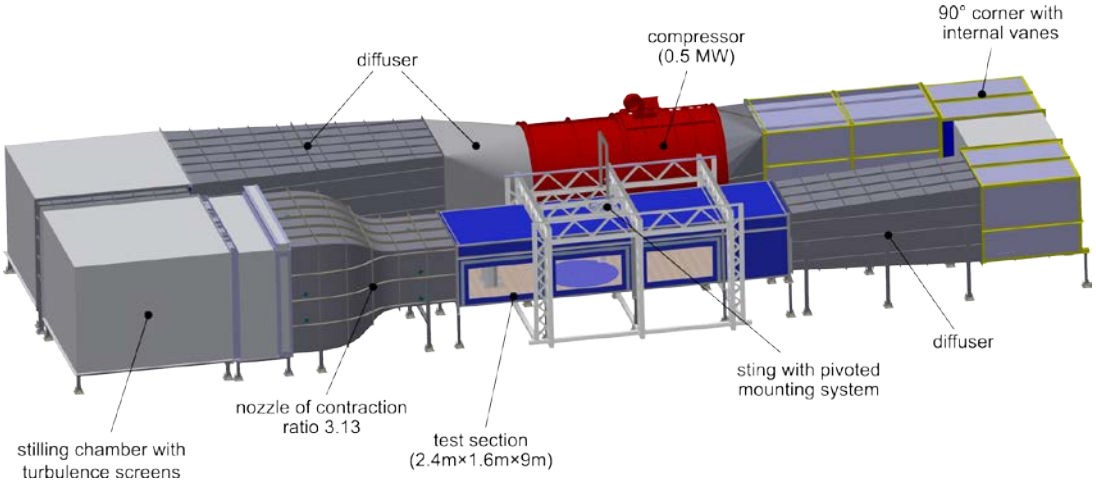

Figure 2: Crosswind simulation facility Göttingen (SWG).

Figure 3 shows the freight train model setup installed on a special splitter-plate in the SWG test-section. The model scale is 1:15 with an overall length of 6.24 m including a modelled single track with ballast and rail. In this measurement setup an 8.4 m long splitter plate was used, which reduces the effective test-section height to 1.15 m. The model consists of a 2410 mm upstream and a 530 mm downstream flow body (black) with a scaled freight train cross-section as well as a modifiable test section (blue) with a test container (dark blue) on a generic freight wagon base (grey). The test container represents a modelled version of the FR8-LAB, a 7.82 m long DLR test container for full-scale measurements in real world operation [4], with scaled dimensions of 521 mm x 170 mm x 195 mm. The modifiable sections (light blue) can be filled with block elements in order to vary the loading gaps up- and downstream of the test container. The filler part length corresponds to increments of the test container length L_c, which provides a range of scaled gaps from 10.4 mm up to 1303.3 mm or 0.156 m up to 19.55 m in full-scale (corresponds to 1/50 L_c up to 2.5 L_c).

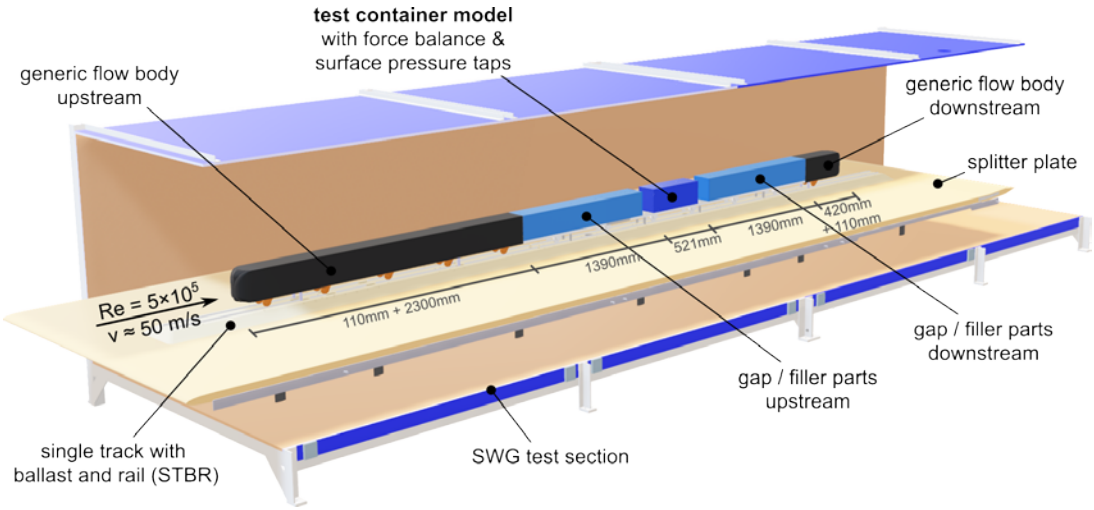

Figure 3: Freight train model setup with single track ballast and rail on a splitter plate in the test-section of the SWG wind tunnel.

The measurements presented in this work were performed at a Reynolds number of 5.5 x 10^5 in relation to the test container width (corresponds to an inflow velocity of approx. 50 m/s). The parameter study was carried out at an angle of attack of 0° and additionally 5° in order to consider the effect of small levels of crosswind. Figure 4 shows the test container model, which was mounted on a six-component strain-gauge balance onto the freight wagon base to provide a decoupled measurement of the aerodynamic drag of the test container only. Furthermore, the test container was equipped with 254 pressure taps around the exposed surface sides to investigate the change in the flow around the test container depending on the up- and downstream gap. This surface pressure tap pattern corresponds to the pressure taps installed in the FR8-LAB. The pressure data will be used in future work to validate and optimize the acquired drag database from wind tunnel tests with full-scale data in real-world operation and comparison with existing results from the literature [5].

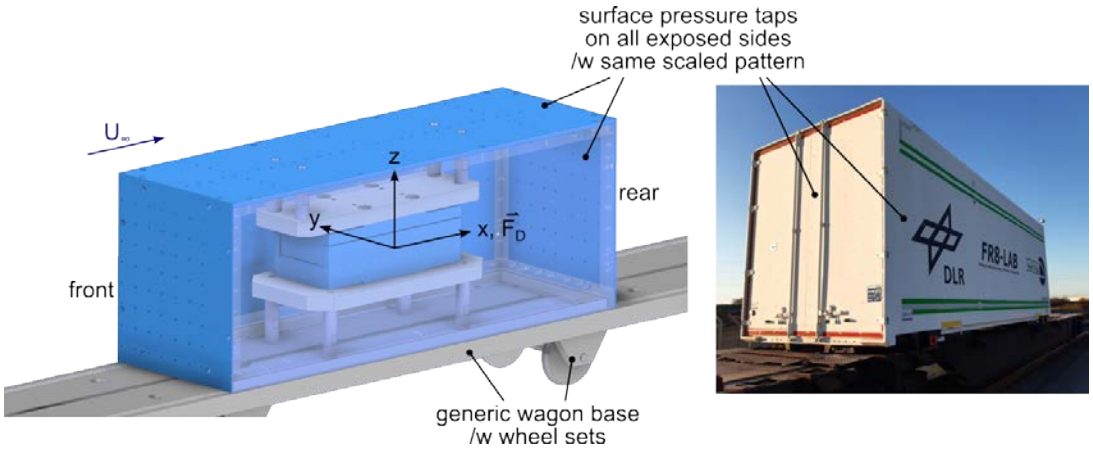

Figure 4: Test container, equipped with 254 surface pressure taps, mounted on a 6-component strain gauge balance attached to the wagon base model plate.

2.2 Study of aerodynamic drag with incremental gap size

From here, all measures are given in full-scale dimension. In the first step, the aerodynamic drag c_D of the test container was measured for selected increments of the upstream gap and a fixed downstream gap of 0.78 m (see Figure 5a). In the second step, vice versa, the downstream gap was varied with the same increments and a fixed upstream gap of 0.78 m (see Figure 5b). These two schemes stretch the main axis of the resulting drag database. A fixed gap of 0.78 m was chosen as an example gap size between containers with 1/10 of the test container length. In the third step, the drag was measured with a combination of different increments for the up- and downstream gaps to analyse the dependency of both gaps on the drag (see Figure 5c).

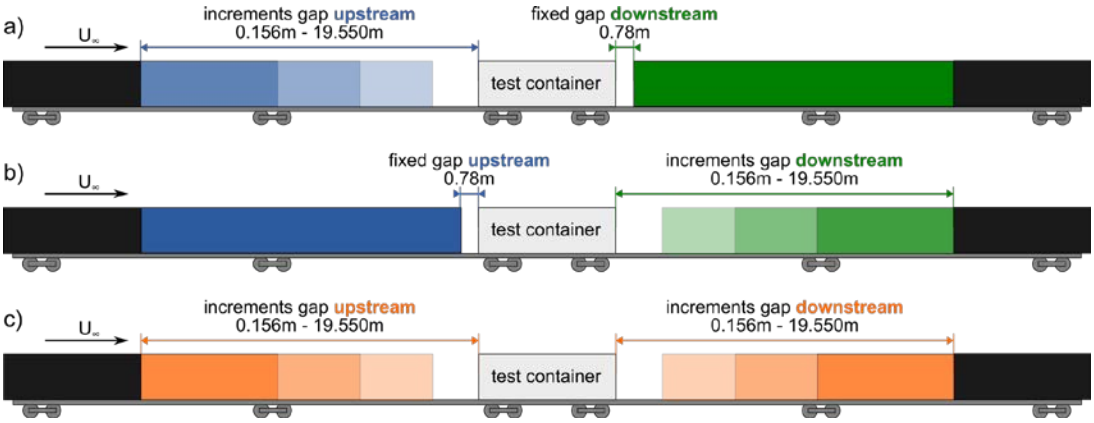

Figure 5: Drag study schemes with a) increments upstream, b) increments downstream, c) combinations of increments upstream and downstream.

To give examples for loading gap ranges of higher interest, four different categories of typical gap were specified using possible loading gaps of two common freight wagon types (W1&2), here: SGMMNS 52' & SGNNSS 80' (see Table 1) loaded with two different types of swap bodies (SB1&2) with 7.45 m and 7.82 m length (see Table 2). The 7.82 m swap body (SB2) corresponds to the swap body type of the FR8-LAB.

	type	length	buffer length	min. distance to load	SB slots
freight wagon W1	SGMMNS 52'	17.35 m	0.665 m	0.065 m	2
freight wagon W2	SGNNSS 80'	25.94 m	0.620 m	0.220 m	3

Table 1: Wagon specifications for W1 and W2.

	type	length	width	height (loaded)
swap body SB1	WK7.3 STG	7.45 m	2.55 m	2.925 m
swap body SB2 (FR8-LAB)	WK7.7 STG	7.82 m	2.55 m	2.925 m

Table 2: Swap body specifications for SB1 and SB2.

The variety of possible loading gaps with the combination of these wagon and swap body types is illustrated in Figure 6. The different gaps are categorized by their occurrence in the loading scheme: ‘CC’ for gaps between containers on the same wagon, ‘WW’ for gaps between containers with an inter-car gap and ‘1ES’ or ’2ES’ for gaps including one or two empty slots. The resulting gap sizes depend on the specifications of the wagon and swap bodies like wagon length, container slots, spigot positions, wagon buffer size, minimum distance to the load and the swap body length. It should be noted, that the WW gaps include the wagon buffers and the minimum distance to the swap bodies (see Table 1), which is determined by the spigot positions.

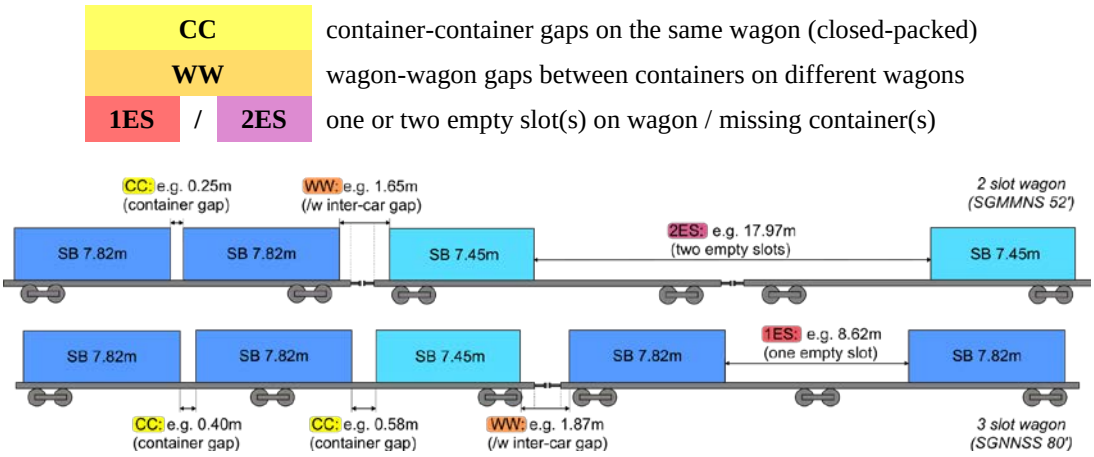

Figure 6: Characterization of gap types in a loading scheme of a freight train.

The drag force $F_{D,i}$ was measured by the force balance in the longitudinal or x-direction of the test container (see Figure 4) at a wind speed U_i^2 on the test container’s cross-section area A. The specific drag coefficient c_D for each gap combination was then calculated by:

$$F_{D,i} = \frac{1}{2} A \rho c_D U_i^2 \Leftrightarrow c_D = \frac{2F_{D,i}}{A \rho U_i^2} \tag{1}$$

With the once determined drag coefficient c_D, it is also possible to calculate the drag force $F_{D,i}$ for other wind or train’s travelling speeds U_i^2, which was used in further analysis to determine the relative increase in energy or work needed, if a container is placed in a specific loading scheme in a realistic operational track profile with varying train speeds. The work needed to move a load with a specific gap-related coefficient c_D was calculated by the sum over all track sections with different train speeds as:

$$\Delta W_D = \sum_i F_{D,i} \cdot \Delta s_i = \frac{1}{2} A \rho c_D \sum_i U_i^2 \cdot \Delta s_i \tag{2}$$

Equation (1) shows, that the drag force $F_{D,i}$ is proportional to the velocity U squared, that means it increases way faster with higher speeds than e.g. the mechanical forces, which are constant or depend linear on the train speed as described by the Davis equation [6].

3 Results

3.1 Aerodynamic drag of a single test container

Figure 7 shows the drag coefficient c_D of the test container as a function of the full-scale loading gap in case of the upstream gap (blue) as illustrated in Figure 5a and in case of the downstream gap (green) as illustrated in Figure 5b at 0° and 5° cross-wind condition. The highlighted areas indicate the example gaps (see Section 2.2) between containers (yellow), wagons (orange) or with one or two empty slots (red, purple).

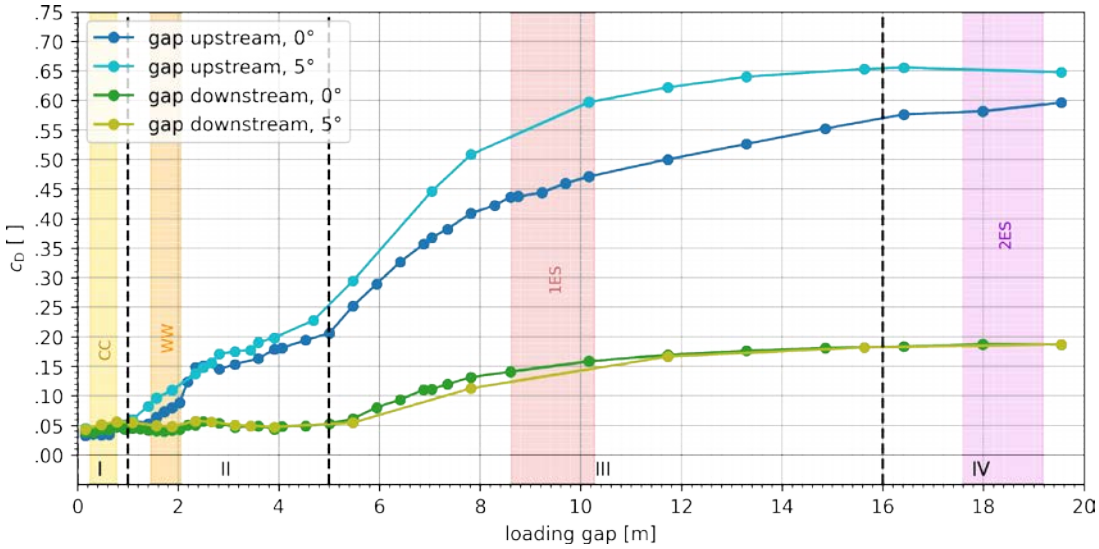

Figure 7: Aerodynamic drag coefficient of test container for gap upstream (cf. Figure 5a) and gap downstream (cf. Figure 5b) at 0° and 5° cross-wind condition.

Four different regimes are evident in Figure 7, labelled with I-IV (dashed vertical lines), with different characteristic dependencies between loading gaps size and drag coefficient. In the following, the observations and the resulting impact for freight train aerodynamics are described for each regime individually (cf. Figure 8 to Figure 11).

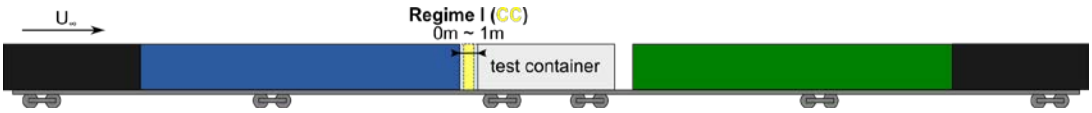

Figure 8: Container-Container-gap in regime I (0 m - 1 m).

Figure 8 shows the range of 0 m to 1 m (regime I) for the upstream gap size. In this regime, the mean aerodynamic drag coefficient of all cases, up- and downstream gap as well as 0° and 5° cross-wind condition, is approximately constant with $c_D \approx 0.043 \pm 0.008$ (cf. Figure 7). A potential explanation could be, that in case of small gap sizes smaller than 1 m, the air is trapped inside of the cavity and the turbulent boundary layer flow does not interact with flow inside of the gap. The gaps in this regime represent typical container-container (CC) gaps between containers on a single wagon without inter-car gaps (cf. Figure 7, yellow). From that follows, that a change of the gaps between loads on a wagon up to about 1m in a close-packed loading

scheme does not significantly increase the total aerodynamic drag of the train. This information can be used by freight wagon manufactures to specify spigot positions dependent on the length of swap body types loaded on the wagon.

Figure 9: Wagon-Wagon-gap in regime II (1 m - 5 m).

Figure 9 illustrates the gap range in regime II of 1 m up to 5 m. Figure 7 shows, that the aerodynamic drag significantly increases from about 0.05 to 0.20 with the size of the upstream gap, while no change is notable with larger downstream gaps. The drag increases almost linear with the upstream gap size and approximately doubled from a 1 m to 2 m gap respectively quadruples for a 4 m upstream gap. This regime includes typical gaps between containers loaded on different wagons including an inter-car gap between two wagons and the minimum distance to the load at each end of a wagon. Here, the wagon-wagon-gaps (WW) for the example wagons and loads represent only a small range at the beginning of this regime (Figure 7, orange). In case of e.g. SB2 the buffer size plus distance to load specifications are quite similar with 1.46 m for W1 and 1.68 m for W2 (cf. Table 1). Therefore, a change between the example wagon types has a minor effect on the aerodynamic drag. But with a more significant change in the WW gaps by using other spigot positions or changing the overall wagon design, the total aerodynamic drag could be reduced down to the drag level in regime I. Recommendations for wagon manufactures would be to minimize the length of buffer size plus minimum distance to load in future freight wagon designs, ideally down to < 1 m. In case of loading logistics, smaller swap bodies or unfavourable spigot positions would mean larger WW gaps, which would lead to a linear increase of the drag of each affected swap body.

Figure 10: One missing container in regime III (5 m - 16 m).

Figure 10 shows the gap range in regime III of 5 m up to 16 m, which includes gaps between loads with one empty slot or missing swap body (1ES, cf. Figure 7, red). The results in Figure 7 shows, that in this gap range the aerodynamic drag increases with a strong, degressive rise in case of the upstream and downstream gap. In this regime, the downstream gap starts affecting the aerodynamic drag of the test container, which indicates the development of a characteristic wake flow behind the container. The additional turbulent structures in the wake flow not only affect the test container, but also the following load, which would explain the strong increase in case of the upstream gap as well. Both progressions show an increase in the drag, which converges to a maximum of about $c_D \approx 0.65$ in case for the upstream gap and $c_D \approx 0.2$ for the downstream gap. The results in this regime emphasize the large impact of empty slots in the loading scheme of a freight train. Not only the missing container itself, but also the additional CC or WW gaps to the next load leads to a higher

sensitivity of the drag dependent on the total gap size. Due to the fact, that every upstream gap is a downstream gap of the previous load, the gaps in this regime are the most important when it comes to the aerodynamic optimization of the loading scheme and reduction of a freight trains energy consumption.

Figure 11: Two missing containers in regime IV (> 16 m).

The fourth and last regime IV represents gaps larger than 16 m (cf. Figure 11). As already mentioned, Figure 7 shows almost a converged progression of the aerodynamic drag in all cases. Gaps larger than 16 m or more than two empty slots (2ES, cf. Figure 7, purple) do not lead to a significant increase in the aerodynamic drag anymore with $\Delta c_D \approx \pm 0.012$. It is assumed, that the load sees an almost free-stream like flow in this case.

The results of the main axis shown in Figure 7 and the combinations of gap increments illustrated in Figure 5c, were combined to determine a full drag database for 0° and 5° cross-wind. Figure 12 shows the visualised results of all measured data with linear interpolation of unmeasured gap combinations.

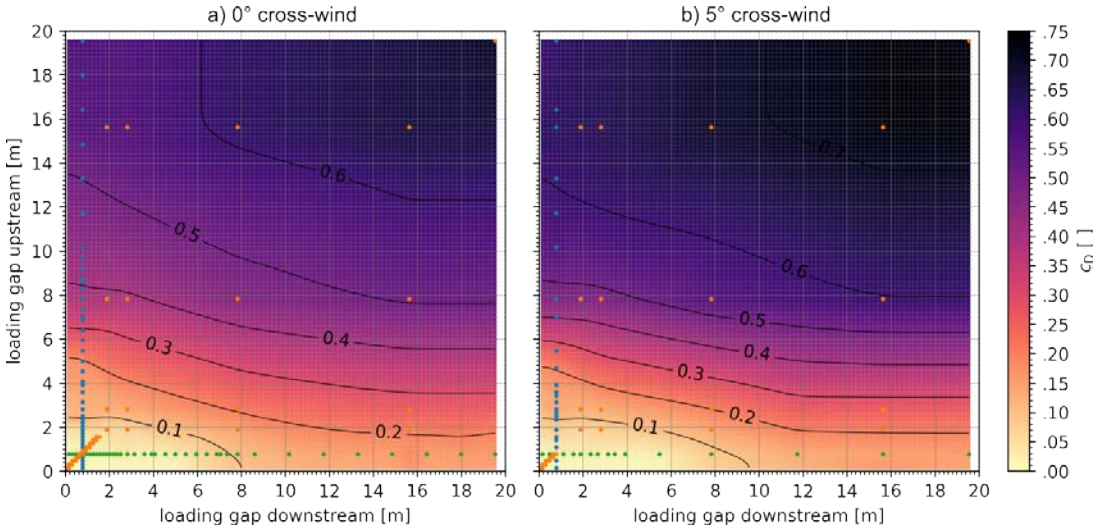

Figure 12: Linear interpolated drag coefficient for up-/downstream gaps around the test container at (a) 0° cross-wind and (b) 5° cross-wind condition.

The loading gap upstream (x-axis) and downstream (y-axis) are given in full-scale. The colormap indicates the value for the drag coefficient from 0 (white) up to 0.75 (black). Further validation and optimization of this database, including boundary layer sensitivity, additional cross-wind analysis and especially the iterative checking with full-scale data from the FR8-LAB under real-world operational conditions, are one of the future parts of this work and will be presented in further publications. At this point, the datasets are used to demonstrate the calculation of the total aerodynamic drag of

the load, the use case for analysing and compare different loading schemes and estimate an energy saving potential with regard to realistic track profiles at different train speeds.

3.2 Effect of loading schemes on total aerodynamic drag

To put the changes of the aerodynamic drag of a single container in perspective of full loading schemes, the presented results were used to calculate the change in total drag between different loading schemes of an example freight train. To demonstrate the capability of the drag database, 11 different loading schemes LS1-LS11, illustrated in Figure 13, were compared. The length of the freight train is determined by the worst-case loading scenario, two empty slots after each loaded swap body, of 24 swap bodies in total. This leads to a freight train length of over 600 m, which corresponds to a typical freight train length operating in Germany. The impact of freight train aerodynamics increases even more with view on current plans for expansions of the railway network for freight trains with a maximum length up to 740 m [7].

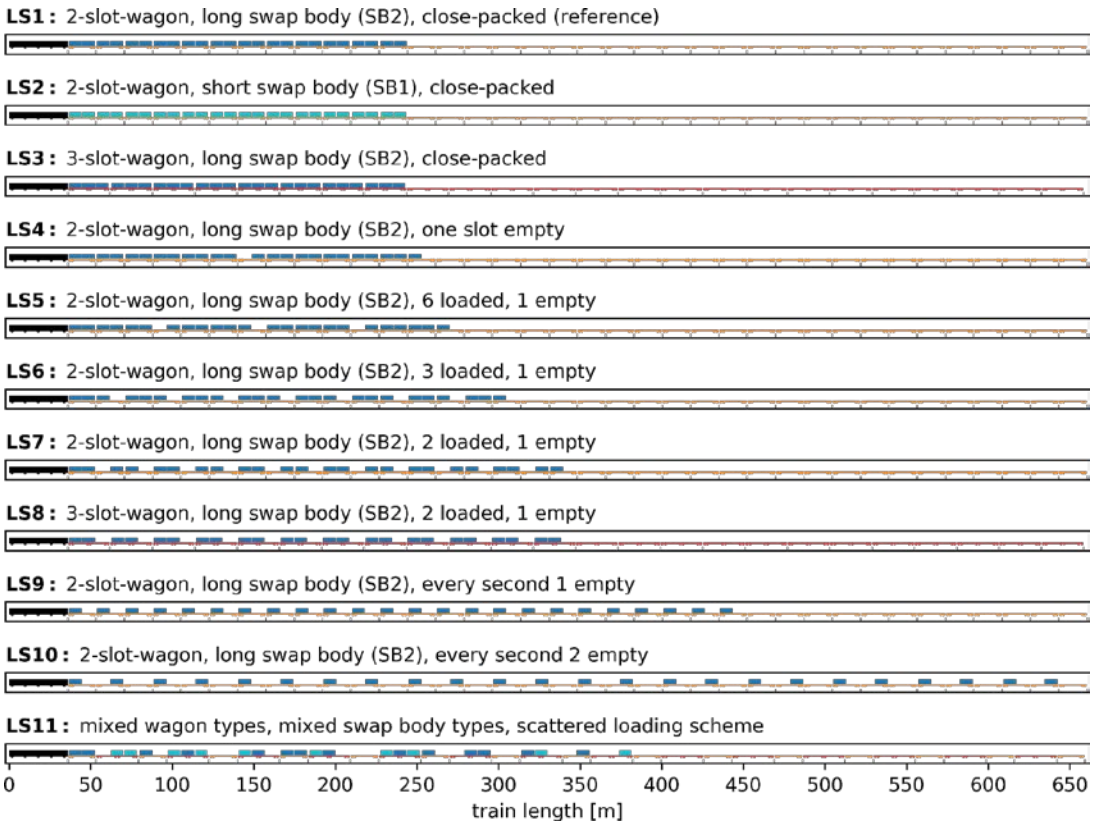

Figure 13: Overview of loading schemes LS1-LS11.

The loading schemes shown in Figure 13 were chosen to represent a systematic increase of loading gaps with empty slots as well as the subdivision in characteristic drag regimes shown in Figure 7. In the frame of this selection, loading scheme 1 (LS1) represents the minimum drag or reference configuration. LS1 is a combination of long swap bodies (SB2, blue) on short wagons (W1, orange) in a close-packed scheme.

LS2 represents the same loading scheme with shorter swap bodies (SB1, cyan) and LS3 with longer wagons (W2, red). The loading schemes LS4-LS10 show loading schemes with one empty slot after 12, 6, 3, 2 and 1 loaded swap body, up to two empty slots after each swap body. These cases are used to demonstrate the range of loading schemes, which are captured by the determined drag databases. The additional loading scheme LS11 represents a randomly scattered case with different wagon and swap body types to include a non-systematic, random, possibly operating freight train loading scheme to compare with the ideal, close-packed case LS1. Figure 14 shows the total increase of the aerodynamic drag for each scheme in relation to LS1.

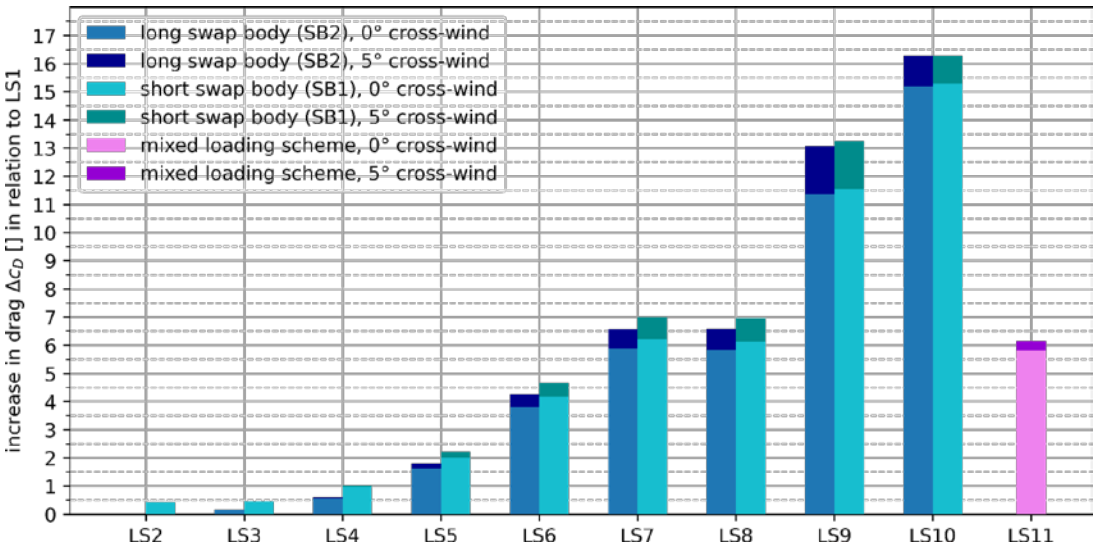

Figure 14: Resulting increase in the aerodynamic drag force in relation to the reference loading scheme LS1 (minimum drag).

The histogram includes the increase in aerodynamic drag for each scheme shown in Figure 13 (blue) as well as the loaded with the shorter swap bodies (C1, cyan) including 0° and 5° cross-wind. As expected from the results presented in section 3.1, the aerodynamic drag increases overall for the case of 5° cross-wind. Further analysis will be done, to include these results into a representative database for real-life operational conditions. Here, only the 0° cross-wind results are used to demonstrate the principle of using this database for further energy and cost estimations.

3.3 Estimations for energy saving potential

In the first step, Equation (1) and (2) were used to calculate the overall increase of energy consumption ΔW_D per increase in drag of $\Delta c_D = 1$ over a 100 km trip at a constant speed of 100 km/h compared to 200 km/h. The increase ΔW_D ranges from 0.1 MWh/100km per Δc_D at 100 km/h up to 0.4 MWh/100km per Δc_D at 200 km/h, which corresponds to a quadrupling due to the quadratic dependency to the train speed U for the drag force (cf. Equation 1). In the second step, the energy savings were estimated for an example track profile of a 300 km trip, shown in Figure 15, with different sections of different operating speeds to include the dependency on the train

speed. Three cases with a maximum speed limit $U_{\max}$ of 120 km/h as in normal operation, 160 km/h as in possibly future high-speed freight operation and 200 km/h as a futuristic high-speed operation, ideally matching with passenger train operation, were compared. The estimated change in energy consumption ΔW_D was calculated per section and train speed. The cumulative, total difference in energy consumption between the loading schemes from Figure 13 is summarized in Figure 16.

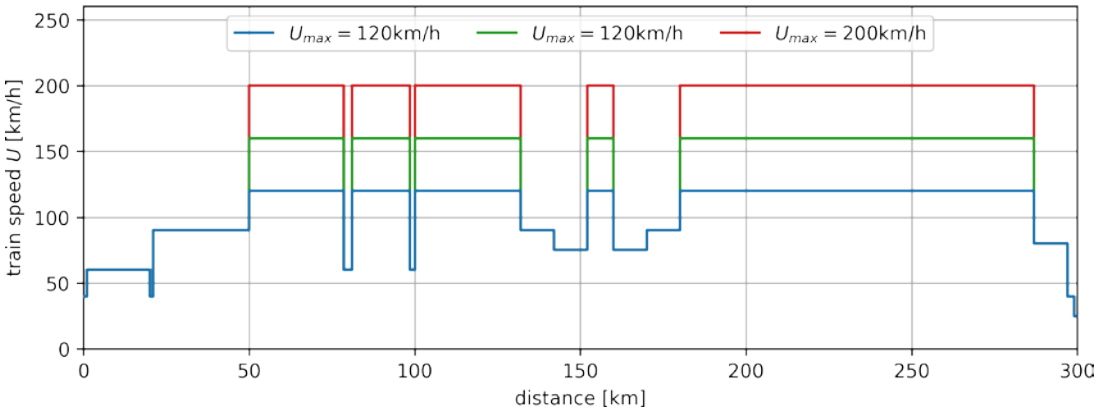

Figure 15: Train speed profiles of test track with max. train speed of 120 km/h, 160 km/h and 200 km/h in max. speed track sections.

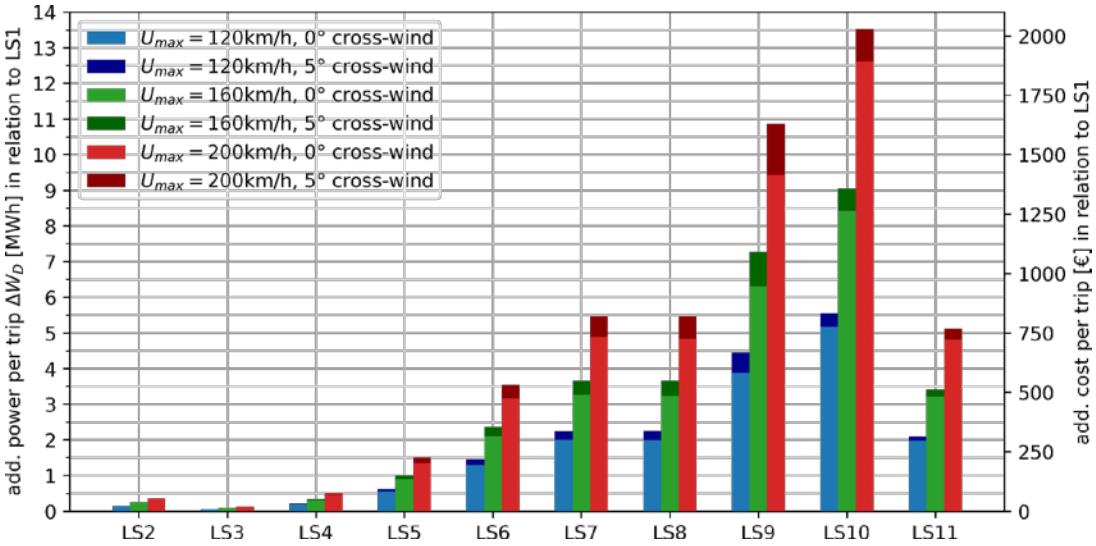

Figure 16: Estimated increase in energy (and cost) consumption for LS2-LS11 in relation to LS1 with regard to the example track profile shown in Figure 14.

Additionally, an estimation of the additional cost with an assumption of 0.15€/kWh is noted on the y-axis at the right-hand side. The results for LS2 and LS3 and the comparison between LS6 vs. LS7 show, that the minor difference in the specifications of the swap bodies SB1 and SB2 or wagons W1 and W2 lead to a minor impact on the energy consumption compared to loading schemes with empty slots as in LS5-LS10. As suggested in section 3.1 the aerodynamic optimization of the close-packed loading schemes is more related to a change in the overall wagon specification in

future high-speed freight wagon designs. The energy saving potential in case of changing from LS11 to LS1 for one 300 km trip at this track speed profile would save nearly 2 MWh or 300 € per trip, which would be even higher considering 5° cross-wind conditions.

4 Conclusions and Contributions

The effect of incremental gap changes in loading schemes of freight trains on the aerodynamic drag has been investigated in a detailed parameter study. The outcome of this work is an incremental database for the aerodynamic drag of a single container loaded on a freight wagon, which provides a calculation of the difference in the total aerodynamic drag between different loading schemes. The results provide an estimation for the total energy saving potential depended on changes in the loading scheme, which then can be used in a cost-benefit calculation by the train operations and directly compare with e.g. logistical cost. In the next steps, the drag data will be refined and validated using further investigations of boundary layer and cross-wind effects, especially with an iterative comparison to the full-scale data acquired by the DLR's FR8-LAB operating under real-world conditions. The comparable pressure measurements in model- and full-scale allow detailed flow investigations. Figure 17 shows a schematic overview of the presented estimation of energy saving potentials and the future integration of the FR8-LAB data as well as actual speed profiles and energy consumption of the freight train the FR8-LAB is loaded on, to improve the presented estimation tool for aerodynamic optimized loading schemes in rail freight transport.

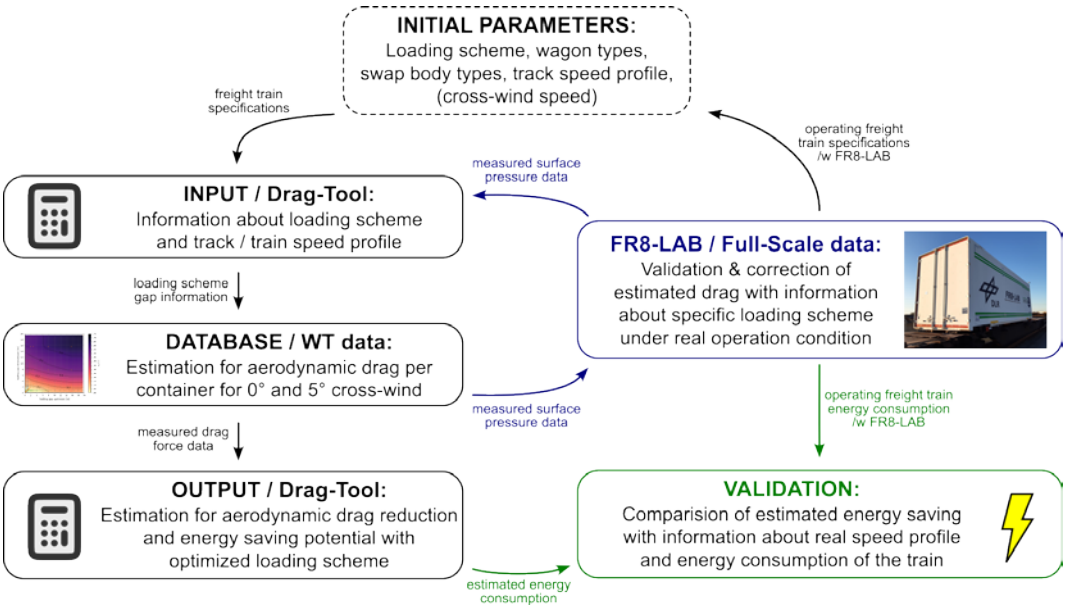

Figure 17: Schematic overview of estimation & optimization loop for the drag database with use of the FR8-LAB full-scale measurements.

Acknowledgements

Funded by the European Union. Views and opinions expressed are however those of the authors only and do not necessarily reflect those of the European Union or the Europe's Rail Joint Undertaking. Neither the European Union nor the granting authority can be held responsible for them. The project is supported by the Europe's Rail Joint Undertaking and its members.

References

[1] Deutsche Bahn AG, "Integrated Report 2022", Berlin, 2022. url: ibir.deutschebahn.com/2022/fileadmin/pdf/db_ib22_e_web.pdf (18/01/2014)

[2] J. Östh, S. Krajnović, "A study of the aerodynamics of a generic container freight wagon using Large-Eddy Simulation", Journal of Fluids and Structures, 44, 31-51, 2014, DOI: 10.1016/j.jfluidstructs.2013.09.017

[3] A.E. Beagles, D.I. Fletcher, "The aerodynamics of freight: approaches to save fuel by optimising the utilisation of container trains", Proceedings of the Institution of Mechanical Engineers, Part F: Journal of Rail and Rapid Transit, 227(6), 635-643, 2013, DOI: 10.1177/0954409713488101

[4] J. Bell, A. Buhr and A. Henning, "Measuring the oncoming flow that operational freight-trains experience using the DLR FR8-LAB", 23rd STAB / DGLR Symposium on New Results in Numerical and Experimental Fluid Mechanics, 23. STAB-DGLR-Symposium 2022, Berlin, Germany, 2022, DOI: 10.1007/978-3-031-40482-5_3

[5] C. Li, D. Burton, M. Kost, J. Sheridan, M.C. Thompson, "Flow topology of a container train wagon subjected to varying local loading configurations", Journal of Wind Engineering and Industrial Aerodynamics, 169, 12-29, 2017, DOI: 10.1016/j.jweia.2017.06.011

[6] B.P. Rochard, F. Schmid, "A review of methods to measure and calculate train resistances", Proceedings of the Institution of Mechanical Engineers, Part F: Journal of Rail and Rapid Transit, 214(4), 185-199, 2000, DOI: 10.1243/0954409001531306

[7] Federal Ministry for Digital and Transport (BMVI), "Rail Freight Masterplan", Rail Freight Masterplan Project Group, Germany, 2017. url: bmdv.bund.de/goto?id=358774 (18/01/2014)